Received: 6 June 2022 | Revised: 17 August 2022 | Accepted: 21 August 2022

DOI: 10.1002/hyp.14684

RESEARCH ARTICLE

WILEY

Impacts of climate and forest management on suspended sediment source and transport in montane headwater catchments

Yang Yang[1] | Mohammad Safeeq[1,2,3] | Joseph W. Wagenbrenner[4] | Asmeret Asefaw Berhe[1,5] | Stephen C. Hart[1,5]

[1]Sierra Nevada Research Institute, University of California, Merced, California, USA

[2]Department of Civil and Environmental Engineering, University of California, Merced, California, USA

[3]Division of Agriculture and Natural Resources, University of California, Davis, California, USA

[4]USDA Forest Service, Pacific Southwest Research Station, California, USA

[5]Department of Life and Environmental Sciences, University of California, Merced, California, USA

Correspondence
Yang Yang, Sierra Nevada Research Institute, University of California, Merced,
463 Sustainability Research and Engineering,
5200 N. Lake Rd. Merced CA 95343, USA.
Email: yyang103@ucmerced.edu

Funding information
National Science Foundation, Grant/Award Numbers: EAR-0725097, 1239521, 1331939

Abstract

Suspended sediment transport in montane headwaters is important to water quality and nutrient balances. However, predictions of sediment source and transport can be difficult, in part, because of a changing climate and increasing frequencies of disturbances. We used observations from 10 headwater streams in water year (WY; starting on 1st October ending on 30th September) 2007–2009 and 2013–2018 to determine the potential impacts of climate and forest management on suspended sediment delivery. We analysed hysteretic responses of suspended sediment for 76 events in five headwater catchments within a snow-dominated site and another five within a lower-elevation, rain-snow transition site, in the mixed-conifer zone of California's Sierra Nevada. Hysteresis patterns were predominantly clockwise at both sites, suggesting localized sediment sources such as streambeds and banks. The warmer, transition site exhibited a lower proportion of clockwise-loop events, faster transport speed and higher peak sediment concentrations than the snow-dominated site. This suggests extended sediment sources and increases in transport can occur as currently snow-dominated areas become rain-snow transitional. Over the nine water years, we observed similar hysteresis effects amongst years under drought, near-average, and extremely wet conditions. Hence, fluctuations in precipitation amounts across years may not influence sediment source area substantially. Furthermore, we compared hysteresis metrics between the control, thin only, burn only and thin combined with burn catchments during the posttreatment period (WY 2013–2018). Hysteresis effects remained unchanged amongst treatments, which may be attributed to the combinations of low-intensity operations implemented with best management practises combined with a four-year drought (WY 2013–2016). Taken together, sediment sources in small headwater catchments will probably remain localized with changing precipitation levels and low-intensity management operations, but it may be extended and potentially lead to higher sediment yields as the main hydrologic input shifts from primarily snow to a mix of rain and snow.

KEYWORDS
climate change, drought, forest thinning, hysteresis analysis, Mediterranean-climate, prescribed fire, Sierra Nevada, soil erosion

1 | INTRODUCTION

Suspended sediment is fine-size organic and inorganic material that remains in the water column whilst water is flowing. In montane headwater basins, suspended sediment is derived from multiple sources, including: channel bed and bank erosion; raindrop splash, sheetwash, rill and gully erosion on hillslopes; erosion from unpaved roads and other disturbed areas; mass movement; and resuspension of in-channel sediment that was previously deposited (Arismendi et al., 2017; Bryan, 2000; Gomi et al., 2005; Leonard et al., 1979). Sediment yields in headwater catchments have often been reported because of their importance to water quality, ecosystem nutrient balances and downstream habitats (Kjelland et al., 2015; Olson & Hawkins, 2017; Stacy et al., 2015, 2019; Yang et al., 2022). Studies of sediment yield alone, however, provide limited information on the source and transport of suspended sediment useful for managing erosion and sediment delivery.

Sediment source and transport behaviour can be evaluated by fingerprinting and tracing sediment (Collins et al., 2017 and 2020), or analysing the hysteresis of suspended sediment concentration (SSC) and discharge (Q; Aich et al., 2014). Compared to the fingerprinting method, hysteresis approach requires fewer chemical analyses and is more often used when high-frequency, paired measurements of SSC and Q are available. The loops often identified in SSC versus Q graphs reflect differences in sediment availability between the rising and falling limbs of the hydrograph, and these graphs have been used to infer the source area. There are four common loop types (Malutta et al., 2020; Williams, 1989): (1) clockwise, which occur when the SSC peak leads the Q peak and imply localized sediment sources; (2) anti-clockwise, which occur when the SSC peak lags the Q peak and imply relatively distant sediment sources; (3) single-valued or linear loop, which occurs when the SSC and Q peak simultaneously, suggesting an unlimited source supply and (4) compound loop (e.g., figure-eight or more complex patterns), which occurs when multiple sediment sources co-exist. Because of the utility of hysteresis analysis, hysteresis metrics have been developed to characterize transport conditions, such as peak values of SSC and Q that describe event intensity, and Hysteresis and Flushing Indices (HI and FI, respectively) that describe the degree and behaviour of the hysteresis effect (Lloyd et al., 2016; Vaughan et al., 2017).

In montane headwater basins, transport of suspended sediment primarily occurs during storm events and snowmelt periods (Wipfli et al., 2007). As the climate continues to warm in many montane areas, snow-dominated regimes will shift towards more rain-dominated regimes (Clifton et al., 2018; Klos et al., 2014; Safeeq et al., 2016). This will increase high-flow events during the wet season (Safeeq et al., 2015; Safeeq et al., 2016), followed by a greater and faster transport of suspended sediment (Ares et al., 2016; Buendia et al., 2016). The reduced snowpack and more frequent freeze–thaw cycles with warmer climates will likely result in more-saturated conditions over the catchment (Henry, 2008; López-Moreno et al., 2017). Consequently, overland flow may increase and transport more sediment from distant areas, which will result in more compound-loop hysteretic events. A warmer climate should also increase the occurrence of severe drought in absolute terms (Diffenbaugh et al., 2015; Williams et al., 2015), and because of the extremely low precipitation, droughts are expected to impact sediment dynamics (Allen et al., 2011). Hence, it is critical to understand how shifting precipitation regimes and changing annual precipitation amounts will impact sediment source and transport in montane regions.

Montane, seasonally dry forests of the western United States (US) will increasingly receive management operations such as forest thinning and prescribed fire to help reduce drought-related tree mortality and wildfire impacts (Agee & Skinner, 2005; Graham, 1999). Those operations can introduce additional soil disturbances that influence sediment supply and transport to nearby streams (Kinoshita et al., 2020; Safeeq et al., 2015). However, inconsistent changes in hysteresis effects (e.g., HI) and transport intensity (peak values of SSC and Q) have been observed following forest thinning (Gomi et al., 2005; Nam et al., 2016) and prescribed fire (Klimas et al., 2020). This has been attributed to variations in operation intensities and precipitation conditions following the treatment. More studies are needed to examine changes in sediment supply and transport following forest management.

Catchment topography can influence sediment source and transport by constraining hydrologic connectivity and flow conditions over the catchment. For example, increases in catchment areas tend to shift the distribution of hysteresis loops from predominately clockwise to a more diverse pattern because of the more extensive and distal sediment source area (Gao & Josefson, 2012; Hamshaw et al., 2018). Catchments with steeper slopes or lower vegetation cover will have higher peak values of SSC and Q and higher FI because of the higher detachment and transport capacity (Haddadchi & Hicks, 2020; Roehl, 1962). Therefore, understanding topographic effects on sediment dynamics can help interpret variations in sediment source and transport amongst catchments.

We conducted hysteresis analysis on 76 single peak events across 10 headwater catchments from water year (WY; starting on 1st October and ending on 30th September) 2007–2009 and 2013–2018 in the mixed-conifer zone of California's Sierra Nevada. All catchments experienced varied precipitation during the study period, ranging from severe drought to extremely wet years. The catchments were evenly distributed between a snow-dominated elevation band and a warmer rain-snow transition elevation band. Catchments in those two elevation bands (hereafter referred to as "sites") were also selectively thinned in 2012 and burned by prescribed fire in 2013 or 2016. We first determined hysteresis metrics for each event and the predominant hysteresis pattern at the two sites. Second, we examined if hysteresis metrics differed between the two sites and between years with different annual precipitation amounts to assess potential climatic impacts on sediment source and transport. Third, we examined the treatment effects on hysteresis metrics to assess impacts of management operations on sediment delivery. Finally, we explored whether hysteresis metrics across the 10 catchments can be predicted by topographic characteristics. Observations and conclusions from this study will help improve our understanding of sediment dynamics

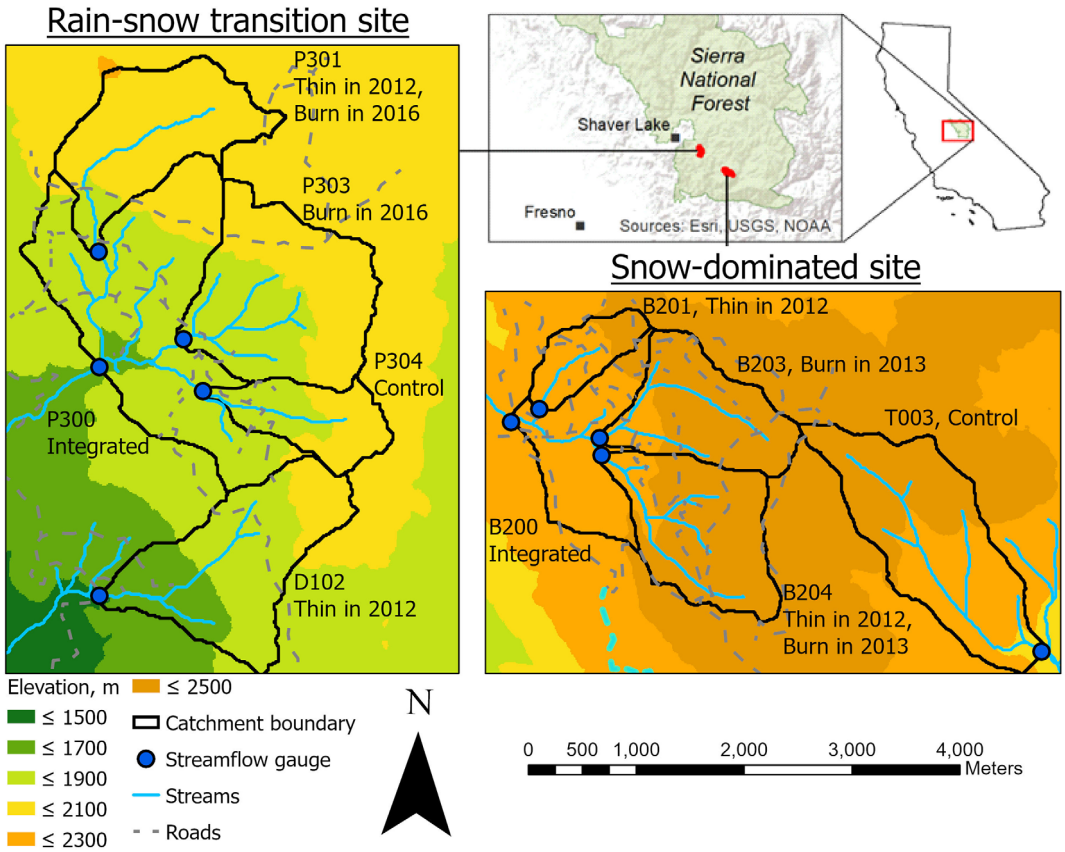

FIGURE 1 Location of five catchments at a lower elevation, rain-snow transition site (Providence Creek; left panel) and another five at a higher elevation, snow-dominated site (Bull Creek; lower right panel) at the Kings River Experimental Watersheds in the Southern Sierra Nevada, California. Elevation is designated by green to brown colours, denoting low to high elevations, respectively. Forest thinning was applied in the summer of 2012 to two catchments at each site (B201 and B204 at the snow-dominated site and P301 and D102 at the rain-snow transition site). Prescribed fire was applied to two catchments at the snow-dominated site (B203 and B204) in the fall of 2013 and two catchments at the transition site (P301 and P303) in the fall of 2016. P304 and T003 were control catchments, and P300 and B200 received integrated effects

in the montane forests in the western US, where ecosystems are experiencing warming and increasing frequencies of disturbance.

2 | MATERIALS AND METHODS

2.1 | Site description

The Kings River Experimental Watersheds are a long-term research area located in the Southern Sierra Nevada in California, USA (Wagenbrenner et al., 2021). The research area experiences a Mediterranean-type climate with an average of 90% of the annual precipitation occurring between October and June (Safeeq & Hunsaker, 2016). It consists of a snow-dominated site at Bull Creek (36°58.631′ N, 119°4.917′ W), where 75%–90% of precipitation falls as snow, and a rain-snow transition site at Providence Creek (37°3.120′ N, 119°12.196′ W), where 35%–60% of precipitation falls as snow (Figure 1a). Both sites have four individual headwater catchments and an integrating catchment in similar ranges of catchment area (ha), mean slope (%), mean aspect (°), relief (m) and drainage density (km km^{-2}; Table 1). Catchments at the snow-dominated site have an elevation range from 2050 to 2490 m, with a mean annual temperature of 7.6°C and mean annual precipitation of 1306 mm y^{-1} (WY 2007–2018; Hunsaker & Safeeq, 2018). Catchments at the transition site have an elevation range from 1485 to 2115 m, with a mean annual temperature of 10.0°C and mean annual precipitation of 1203 mm y^{-1} (WY 2007–2018; Hunsaker & Safeeq, 2018). Dominant soil series at the two sites are Shaver, Cagwin, and Gerle–Cagwin (Johnson et al., 2011). The Cagwin series, classified as loamy coarse sand, mixed, frigid dystric xeropsamments, is most prominent at the snow-dominated site (67%–98% coverage). The Shaver series, classified as coarse-loamy, mixed mesic Pachic Xerumbrepts, is most prominent at the transition site (48%–66%). The Gerle series is classified as coarse-loamy, mixed, frigid Typic Xerumbrepts (Johnson et al., 2011). Overstory vegetation is dominated by red fir (*Abies magnifica* A. Murray bis) and white fir (*Abies concolor* [Gordon] Lindl. ex Hildebr.) at the snow-dominated site, and by white fir and incense cedar (*Calocedrus decurrens* [Torr.] Florin) at the transition site (Lydersen et al., 2019).

In summer 2012, thinning treatments were applied in two catchments each at the snow-dominated (B201, B204) and transition sites

TABLE 1 Catchment characteristics at the Kings River Experimental Watersheds in the Southern Sierra Nevada, California (adapted from Safeeq & Hunsaker, 2016). Catchments are ordered from the highest to the lowest mean elevation

Site	Catchment	Treatment	Mean elevation (m)	Catchment area (ha)	Mean slope (%)	Mean aspect (°)	Relief (m)	Drainage density (km km^{-2})	Mean normalized difference vegetation index
Snow-dominated, *Bull Creek*	B203	Burn	2373	138	18	235	303	4.6	0.46
	B204	Thin & burn	2365	167	17	235	289	5.0	0.49
	T003	Control	2289	228	24	142	414	5.5	0.63
	B201	Thin	2257	53	18	228	225	6.0	0.54
	B200	Integrate	2122	474	18	231	367	5.2	0.51
Rain-snow transition, *Providence Creek*	P301	Thin & burn	1979	99	19	208	318	7.4	0.61
	P303	Burn	1905	132	20	233	292	7.4	0.69
	P304	Control	1899	49	22	249	213	6.9	0.69
	P300	Integrate	1883	461	21	223	424	7.4	0.68
	D102	Thin	1782	121	27	246	491	10.1	0.69

(P301, D102). Thinning treatments in mature stands were conventional timber harvest (i.e., chainsaw-felling, slash left in the stand, logs skidded to a landing) that removed trees across all diameter classes and reduced basal area from 44–79 m^2 ha^{-1} to 27–55 m^2 ha^{-1} (target basal areas varied by predetermined aspect and topographic position classes; Lydersen et al., 2019). California black oak (*Quercus kelloggii* Newb.), sugar pine (*Pinus lambertiana* Douglas) and ponderosa pine (*Pinus ponderosa* Lawson) were retained preferentially. Trees removed from USDA Forest Service land had a maximum diameter at 1.4 m height (i.e., diameter at breast height, DBH) of 76 cm. The thinned watersheds at the transition site contained some privately-owned land, and in these areas some trees with a DBH up to 117 cm were removed. Thinning treatments in young (<30 year old) and even-aged stands were pre-commercial, and shrub cover was reduced to below 10% by mastication in stands with shrub cover >50%. Approximately 10%–25% of the area planned for thinning (or mastication) within thinned watersheds, especially in D102, was excluded from operation due to slope steepness (generally >30% slope) and lack of existing roads.

Prescribed fire was applied to two catchments at the snow-dominated site (B203 and B204) during 18 October 2013–19 November 2013. Burning in the two catchments at the transition site (P301 and P303) was delayed until 14–16 November 2016 due to unfavourable burn conditions. Backing fire, along with some flanking and small runs of head fire, were used at both sites to consume surface and ground fuels with no effect on forest structure. Maximum flame lengths ranged from 1.2 to 1.8 m and burn-day wind speeds were less than 4.5 m s^{-1} at both sites. Details of prescribed fire operation and documentation of soil burn severity and postfire vegetation composition can be found in Lydersen et al. (2019). The thinning and burning treatments generated a thin only, burn only, thin and burn and control treatment catchment at each site. The integrating catchment at the snow-dominated site (B200) received effects from a thin only, burn only and thin combined with burn, and the integrating catchment at the transition site (P300) received effects from a control, burn only and thin combined with burn (Figure 1). The thin, burn and combined thin and burn treatments resulted in relatively low impacts on soils and basal area (Lydersen et al., 2019). USDA Forest Service best management practises (USDA, 2011) were followed during implementation of treatments.

2.2 | Sample measurements and hysteresis analysis

We measured Q (L s^{-1}) using a weir at the outlets of two catchments (P300 and T003), a stage-discharge rating curve in B200, and a small and large Montana-style Parshall flume in each of the other seven catchments (Hunsaker et al., 2012; Hunsaker & Johnson, 2017; Wagenbrenner et al., 2021). Stage was recorded at each rating section using a pressure transducer, and turbidity was measured just upstream of the rating section with a turbidimeter (Wagenbrenner et al., 2021). Suspended sediment samples were collected using ISCO 6712 automated samplers (Teledyne ISCO, Lincoln, NE, US) at the outlets of each catchment, upstream from the weir, small flume, or stream gauge (Hunsaker et al., 2007). The ISCOs were triggered to sample water every 15 to 30 min when the discharge rate and turbidity were above preset thresholds (Hunsaker et al., 2007). Discharge and turbidity thresholds were periodically adjusted to account for seasonal variations (i.e., thresholds were higher in winter and lower in summer). Water samples were processed for SSC (mg L^{-1}) using vacuum filtration with 1 μm glass fibre filters. Precipitation at 15-min intervals were measured using Alter-shielded weighing bucket precipitation gauge (Belfort 5–780 weighing rain gage, Baltimore, MD, USA and 260–952 Alter-style wind screen, Novalynx Corporation) at four locations, two each at the snow-dominated and rain-snow transition site (Wagenbrenner et al., 2021).

We analysed 76 runoff events that included Q and SSC for a single peak and a record for the complete rising and falling limbs of each event (Appendix A, Table A1). For each event, we first graphed SSC as a function of Q to determine the corresponding hysteresis loop type.

We then determined the minimum value, maximum value, and speed of Q and SSC (i.e., Q_{min}, SSC_{min}, Q_{max}, SSC_{max}, Q_{speed}, and SSC_{speed}) for each event. The Q_{speed} and SSC_{speed} were defined as the difference between the maximum and minimum values divided by the time between their occurrences. We report the Q_{min}, SSC_{min}, Q_{max}, SSC_{max}, Q_{speed} and SSC_{speed} as the unit-area values because of differences in area amongst the catchments and these indices are often sensitive to catchment area (Gao et al., 2013; Park et al., 2019). We also calculated the lag time (min), defined as the time between SSC_{max} and Q_{max}.

To calculate the HI and FI of each event, we first normalized the Q and SSC to reduce the influence of differences in Q and SSC amongst events:

$$Q_{i,norm} = \frac{Q_i - Q_{min}}{Q_{max} - Q_{min}}, \quad (1)$$

$$SSC_{i,norm} = \frac{SSC_i - SSC_{min}}{SSC_{max} - SSC_{min}}, \quad (2)$$

where Q_i and SSC_i are the discharge and suspended sediment concentration (respectively) at time step i, Q_{min} and Q_{max} are the minimum and maximum discharge values (respectively), and SSC_{min} and SSC_{max} are the minimum and maximum sediment concentrations (respectively). We then calculated the sediment concentration at 2% intervals of normalized discharge for both rising and falling limbs, using interpolated linear regressions based on the two adjacent pairs of $SSC_{i,norm}$ and $Q_{i,norm}$ (Lloyd et al., 2016; Vaughan et al., 2017). The overall HI of one event was the mean of HI at all normalized discharge intervals (2%):

$$HI = \text{mean}\left[SSC^{rising}_{i,norm}(Q_{i,norm}) - SSC^{falling}_{i,norm}(Q_{i,norm})\right] i \text{ for } Q_{i,norm} \in [0.02, 1]. \quad (3)$$

The HI was scaled from −1 to 1 with negative values indicating anticlockwise loops (i.e., inferring distant sediment source) and positive values indicating clockwise loops (i.e., inferring localized sediment source; Vaughan et al., 2017). We calculated the FI of one event by subtracting the normalized sediment concentration at the beginning of the event ($Q_{i,norm} = 0$) from that at the peak of the event ($Q_{i,norm} = 1$). The FI was also scaled from −1 to 1 with negative values indicating a diluting effect (i.e., decreases in SSC on the rising limb, inferring source limited) and positive values indicating a flushing effect (i.e., increases in SSC on the rising limb, inferring transport limited; Vaughan et al., 2017).

2.3 | Statistical analysis

All statistical analyses were conducted in SAS 9.4 (SAS Institute, Inc., 2013). We used a priori alpha level of 0.10 to evaluate statistical significance because of the greater variation typically found in field studies and the limitation of setting thresholds at 0.05 (Amrhein et al., 2019). We first determined median value and interquartile range (IQR, the difference between the lower 25% and upper 25% quartiles) for each hysteresis metric due to their strongly skewed distributions. Hysteresis metrics included: unit-area Q_{min}, Q_{max}, Q_{speed}, SSC_{min}, SSC_{max}, and SSC_{speed}, lag time, HI, and FI. A Spearman's rank-order test was used to explore correlations between hysteresis metrics ($n = 76$ events).

We examined the impacts of precipitation regimes and annual precipitation levels on hysteresis metrics using a nonparametric aligned rank transformation test with repeated measures based on all events. We grouped the WYs that received similar amounts of annual precipitation to increase the statistical power, and classified them as an "average year" when annual precipitation was between 1046 and 1323 mm (WY 2008, 2009, 2016, and 2018, $n = 27$), a "dry year" when average precipitation was less than 1046 mm (WY 2007, 2013, 2014, and 2015, $n = 36$), and a "wet year" when average precipitation was greater than 1323 mm (WY 2017, $n = 13$; Appendix A, Figure A1). Independent class variables were *site* with *Catchment* nested within *site* and *classified year* (average, dry, or wet). The interaction of *site* and *classified year* was not significant for all hysteresis metrics (data not shown), hence was not included in any of the models.

We examined the forest treatment effects on hysteresis metrics at each site using the aligned rank transformation test with repeated measures. The Dunn's post-hoc test was used to compare between groups when the null hypothesis of no effect was rejected. At the snow-dominated site, we used measurements from the four treated catchments (thin only, burn only, thin combined with burn, and control (WY 2013–2018)). At the transition site, we only included posttreatment measurements from the two catchments (thin only and control) because of the limited number of observations at burn only ($n = 2$) and thin combined with burn (1) catchments. The two integrating catchments (i.e., B200 and P300) were not included in the analysis because the delayed prescribed fire resulted in an inconsistent integrating effect across repeated measures. We did not compare treatment effects on hysteresis metrics at each site between different classified years because datasets were not available for all three classified years (Appendix A, Table A1).

We applied regression analyses with linear, exponential and quadratic functions to examine if variability in the median values of the hysteresis metrics across catchments and time was explained by topographic characteristics ($n = 10$ catchments). Independent variables were mean elevation, catchment area, mean slope, mean aspect, relief, drainage density and mean normalized difference vegetation index (Table 1). Mean elevation, catchment area, mean slope, mean aspect and relief (the difference in elevation between the highest and lowest locations) were derived using a 30-m digital elevation model obtained from U.S. Geological Survey repository (http://nationalmap.gov/viewer.html). Drainage density was digitized from U.S. Geological Survey topographic maps and calculated by overlaying the stream network layer on each catchment boundary. Mean normalized difference vegetation index was calculated based on the Moderate Resolution Imaging Spectrometer (MODIS) 250-m NDVI data for water years 2004–2014 (MYD13Q1 version 5). In each case, we chose the model

with the lowest AICc (the Akaike information criterion [AIC] that corrects for small sample sizes). A simpler model (i.e., linear) was chosen if two models had AICc values that differed by less than 2 (Burnham & Anderson, 2002). We log-transformed the hysteresis metrics for regression analyses to meet the assumption of normality and homoscedasticity of the residuals.

3 | RESULTS

3.1 | Overall hysteresis patterns and metrics

Four types of hysteresis pattern were observed from the 76 single peak events, namely, clockwise (68), anticlockwise (2), figure-eight with a clockwise-anticlockwise-clockwise pattern (4), and non-hysteretic pattern (single-valued loops, 2; Figure 2). The clockwise-loop events were prevalent at both sites: 94% at the snow-dominated site and 86% at the rain-snow transition site (Figure 3). The median ± IQR of 76 events were 0.15 ± 0.23 L s^{-1} ha^{-1} for Q_{min}, 0.34 ± 0.72 L s^{-1} ha^{-1} for Q_{max}, 0.08 ± 0.14 L s^{-2} ha^{-1} for Q_{speed}, 0.06 ± 0.16 mg L^{-1} ha^{-1} for SSC_{min}, 0.67 ± 1.42 mg L^{-1} ha^{-1} for SSC_{max}, 0.22 ± 0.56 mg L^{-1} s^{-1} ha^{-1} for SSC_{speed}, −30 ± 44 min for lag time, 0.42 ± 0.29 for HI and 0.52 ± 0.68 for FI (Table 2).

The Spearman's rank-order correlation test revealed that Q_{min}, Q_{max}, and Q_{speed} were positively correlated between each other, and SSC_{min}, SSC_{max} and SSC_{speed} were also positively correlated between each other ($p < 0.01$, $r \geq 0.56$, $n = 76$; Figure 4). SSC_{min} was positively correlated with Q_{min} ($p = 0.07$, $r = 0.21$) and lag time ($p = 0.09$, $r = 0.20$). SSC_{max} was positively correlated with Q_{max} ($p = 0.07$, $r = 0.21$) and Q_{speed} ($p = 0.05$, $r = 0.22$). HI was negatively correlated with SSC_{max} ($p = 0.09$, $r = -0.20$), lag time ($p < 0.01$, $r = -0.52$) and FI ($p < 0.01$, $r = -0.58$). FI was positively correlated with lag time ($p < 0.01$, $r = 0.67$; Figure 4).

3.2 | Variations in hysteresis metrics between sites, years and treatments

Comparing hysteresis metrics between the two sites, Q_{speed} and HI were higher, and SSC_{min}, SSC_{max} and SSC_{speed} were lower at the snow-dominated than transition site ($p \leq 0.03$; Figure 5). Q_{min}, Q_{max}, lag time and FI did not differ between the two sites ($p \geq 0.14$; Figure 5).

Comparing hysteresis metrics between classes of water years, Q_{min} and Q_{max} were higher in the wet year compared to average and dry years ($p = 0.05$ and 0.02, respectively; Figure 5). Conversely, SSC_{speed} was higher in dry years compared to average and wet years ($p = 0.03$; Figure 5). There were no differences in Q_{speed}, SSC_{min}, SSC_{max}, lag time, HI and FI amongst the three classes of water years ($p \geq 0.20$; Figure 5).

At the snow-dominated site, the catchment that received forest thinning with no prescribed fire had higher SSC_{min}, SSC_{max} and SSC_{speed} than the control catchment ($p \leq 0.02$; Figure 6); catchments that received prescribed fire only or forest thinning combined with prescribed fire had similar SSC_{min}, SSC_{max}, and SSC_{speed} compared to the control. At the transition site, the catchment that received forest thinning only had lower SSC_{min} ($p = 0.05$) and similar SSC_{max} and SSC_{speed} ($p \geq 0.19$) compared to the control catchment (Figure 6). All the rest of the hysteresis metrics (i.e., Q_{min}, Q_{max}, Q_{speed}, lag time, HI and FI) were similar between the control and treated catchments at both sites ($p \geq 0.12$, Figure 6).

3.3 | Topographic influences on hysteresis metrics

Regression analyses were used to explore if hysteresis metrics were explained by topographic characteristics, including elevation, catchment area, slope, aspect, relief, drainage density, and normalized difference vegetation index. Across the 10 catchments, unit area SSC_{min}, SSC_{max} and SSC_{speed} decreased exponentially with greater catchment areas ($p < 0.01$ and $R^2 \geq 0.72$, Figure 7). Relationships between those SSC metrics and relief were best fit with quadratic functions ($p < 0.01$, $R^2 \geq 0.75$, Figure 7). Unit area SSC_{min}, SSC_{max}, and SSC_{speed} initially decreased and then increased with higher catchment relief, with break points estimated at 375, 384, and 382 m, respectively. However, Q_{min}, Q_{max}, Q_{speed}, lag time, HI and FI across the 10 catchments were not predicted by any topographic characteristics ($p \geq 0.24$, data not shown).

4 | DISCUSSION

4.1 | Hysteretic response of suspended sediment in montane headwater catchments

We observed 89% of the events exhibited a clockwise-loop pattern at the two sites, suggesting a localized sediment source in headwater catchments in the Southern Sierra Nevada. In the central and northern Sierra Nevada, the predominance of clockwise hysteresis pattern has also been observed in headwater catchments and sub-watersheds (Langlois et al., 2005; Martin et al., 2014). Those observations suggest that streambeds and banks, rather than hillslopes, are the main sediment sources in mixed-conifer forests in the headwaters of California's Sierra Nevada. Because variations in HI across our 10 catchments were not explained by catchment area, catchment area may not affect sediment source within the range of areas at our sites. In other montane headwaters catchments of similar size, hysteresis patterns are also often predominantly clockwise (e.g., 3 km^2 for Seeger et al., 2004; 5 km^2 for Pagano et al., 2019; 9 km^2 for Tsyplenkov et al., 2020; 12 km^2 for Fang et al., 2015). In larger catchments, hysteresis patterns become predominantly anticlockwise partially because of the more extensive sediment source area (e.g., 35 km^2 for Esteves et al., 2019; 85 and 230 km^2 for Mano et al., 2009; 499 km^2 for Pagano et al., 2019). Thus, responses of sediment source to catchment area may exhibit a threshold

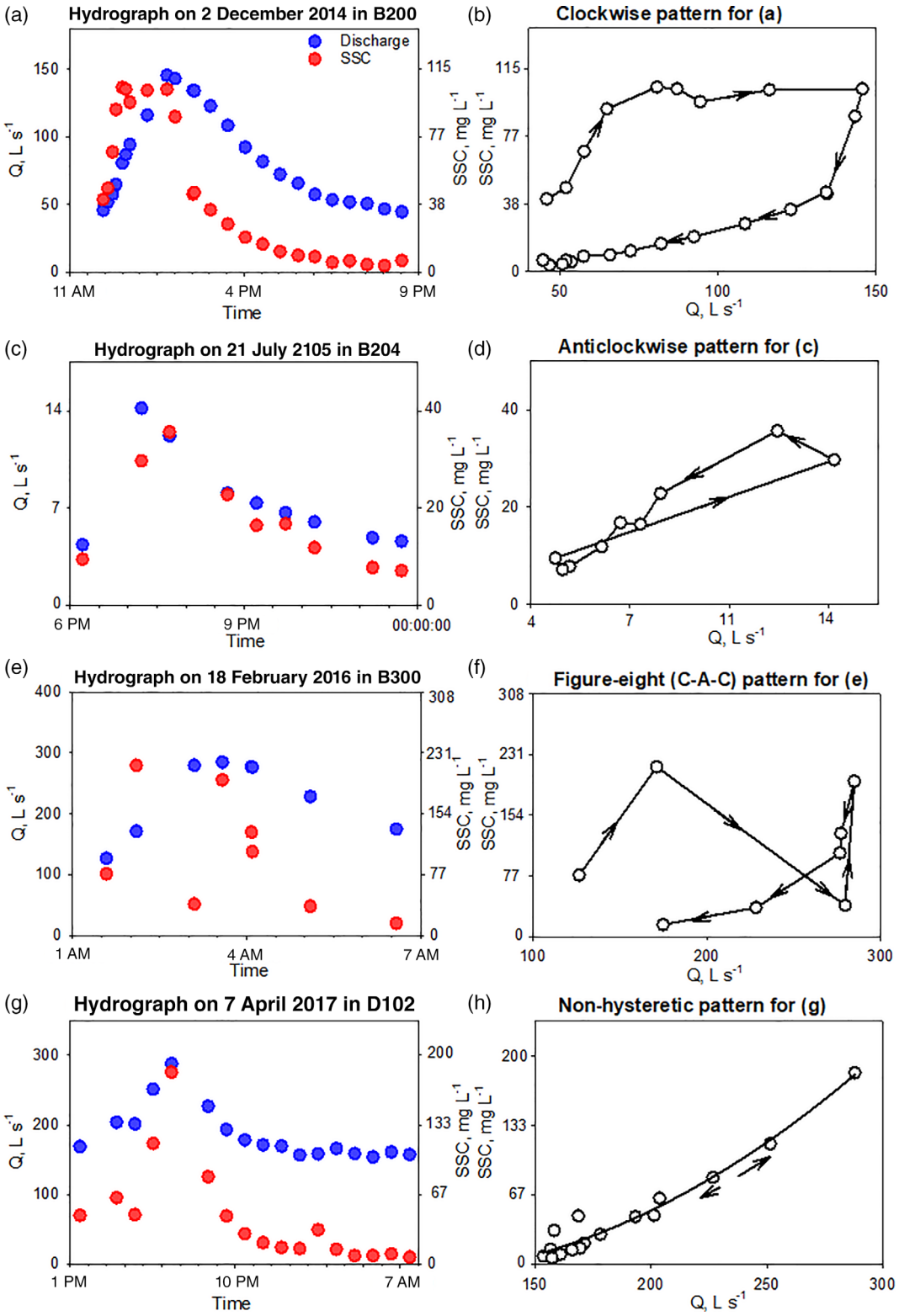

FIGURE 2 Examples of hysteresis relationships between suspended sediment concentration (SSC) and discharge (Q) at the Kings River Experimental Watersheds. Four hysteresis patterns were observed, including a clockwise (a and b), anticlockwise (c and d), clockwise-anticlockwise-clockwise figure-eight (e and f), and non-hysteretic pattern (single-valued pattern bending upwards; g and h)

behaviour: sediments are derived primarily from near-stream areas in smaller catchments but also originate from hillslope locations if catchment area increases to a certain larger size.

Not all events in our study exhibited a clockwise hysteresis pattern, suggesting multiple sediment source areas will occasionally occur in headwater catchments in the Southern Sierra Nevada. Across the

10 catchments over nine WYs, we observed two events that exhibited an anticlockwise hysteresis pattern: one in summer (21 July 2015, B203, 28 mm total event rainfall) and the other in the fall (27 November 2017, P303, 49 mm total event rainfall). In other studies, anticlockwise-loop hysteresis events that occurred in summer dry season have been attributed to relatively large rainfall and fast flow rates on dry soils that extends the hillslope sediment transport (Buendia et al., 2016; Eder et al., 2010; Haddadchi & Hicks, 2021). However, this was not the case in this study, as the anticlockwise-loop event in July 2015 occurred during a relatively low flow event (Q_{speed} = 0.06 L s^{-2} ha^{-1}, as compared to the median value of 0.08 L s^{-2} ha^{-1}). Our summer anticlockwise-loop event may have been due to the storm event, with an average rainfall of 32 mm, that occurred 10 days prior (Appendix A, Table A1), which may have depleted in-channel storage and increased soil moisture within the catchment. Therefore, more sediment was transported from primarily hillslope positions due to the antecedent wet condition. Similarly, anticlockwise-loop events that occurred in the fall in other studies have been attributed to an extreme soil moisture condition that introduced sediment transport from the whole catchment area (Seeger et al., 2004; Williams, 1989). Similarly, our anticlockwise-loop event in November 2017 may have been due to a high-moisture condition that allowed transport of sediment from distal unpaved roads (Stafford, 2011). Storms occurred on this day and also 10 days prior (49 mm total event rainfall on 17 November 2017). The two anticlockwise-loop events in our study were probably not caused by forest thinning and prescribed fire as the treatments had negligible effects on sediment source area (Lydersen et al., 2019) and precipitation on those dates occurred regionally.

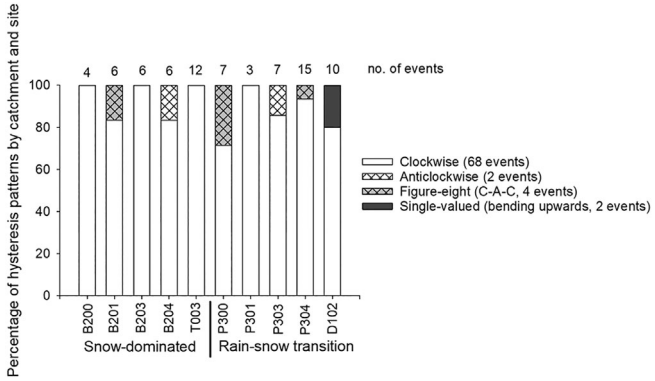

FIGURE 3 Distribution of hysteresis patterns (from 76 total events) in five catchments at a higher elevation, snow-dominated site (Bull Creek) and another five at a lower elevation, rain-snow transition site (Providence Creek) at the Kings River Experimental Watersheds in the Southern Sierra Nevada, California

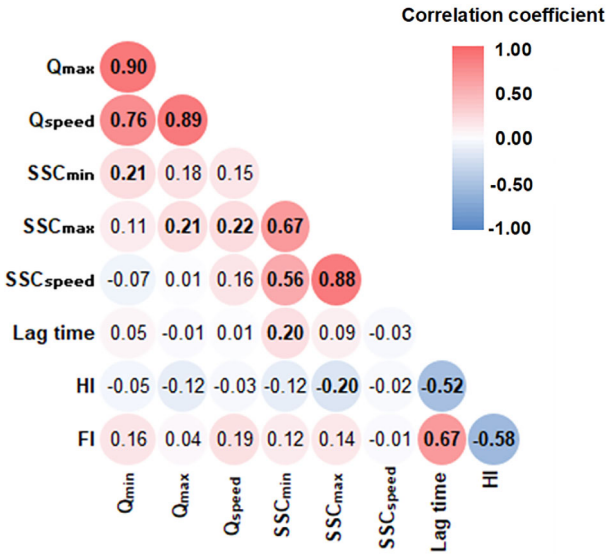

FIGURE 4 Correlations between hysteresis metrics based on all 76 events at the Kings River Experimental Watersheds in the Southern Sierra Nevada, California. Correlation coefficients were estimated using Spearman rank tests and coloured based on their magnitudes and directions. Bolded values were statistically significant ($\alpha = 0.10$)

TABLE 2 Minimum (min), maximum (max), mean, median and standard deviation (SD) levels of hysteresis metrics for 76 single peak events at the snow-dominated and rain-snow transition site from water year 2007–2009 and 2013–2018 at the Kings River Experimental Watersheds in the Southern Sierra Nevada, California

	Hysteresis metrics[a]								
	Lag time, min	Q_{min} (L s^{-1} ha^{-1})	Q_{max} (L s^{-1} ha^{-1})	Q_{speed} (L s^{-2} ha^{-1})	SSC_{min} (mg L^{-1} ha^{-1})	SSC_{max} (mg L^{-1} ha^{-1})	SSC_{speed} (mg L^{-1} s^{-1} ha^{-1})	HI	FI
Min	−120	0.01	0.02	0.01	0.01	0.06	0.01	−0.32	−0.68
Max	120	1.85	4.80	0.46	1.04	11.07	4.40	0.81	1.00
Mean	−34	0.27	0.73	0.12	0.16	1.84	0.63	0.38	0.48
Median	−30	0.15	0.34	0.08	0.07	0.80	0.24	0.42	0.52
SD	46	0.38	0.98	0.11	0.23	2.72	0.94	0.24	0.41

[a]Hysteresis metrics include the unit-area minimum, maximum, and speed of discharge and suspended sediment concentration (i.e., Q_{min}, Q_{max}, Q_{speed}, SSC_{min}, SSC_{max}, and SSC_{speed}), lag time (defined as the time between SSC_{max} and Q_{max}), hysteresis index (HI) and flushing index (FI; see text for HI and FI calculations). The Q_{speed} and SSC_{speed} were defined as the difference between the minimum and maximum values divided by the time between their occurrences.

Four events exhibited a figure-eight hysteresis pattern (i.e., a clockwise followed by an anticlockwise loop), which implies a switch from localized to distant sediment source that provides a continuous sediment source even during the hydrograph recession (Gao & Josefson, 2012; Seeger et al., 2004). One figure-eight event occurred in the winter (18 February 2016, P300) and another occurred in early spring (7 April 2018, P304); the other two both occurred in the fall (31 October 2014, B201 and 28 October 2016, P300). In our study, the mechanism for generating a clockwise loop followed by an anti-clockwise loop is unclear. In other studies, figure-eight events have been attributed to an ice breakup (Williams, 1989) or a mid-storm bank failure (Fan et al., 2012; Stafford, 2011) that increases erosive capacity and sediment concentration sharply. Consequently, in-channel storage is depleted, and sediment sources transition to hillslope locations. We also observed two non-hysteretic events, suggesting a continued sediment supply from stream banks or erosion from distal sources that occurred before the exhaustion of localized sediment. In montane headwater catchments, substantial temporal variabilities in hydro-meteorological conditions introduce dynamic sediment sources (Duvert et al., 2011; Zabaleta et al., 2007).

4.2 | Impacts of precipitation regimes and annual precipitation levels on sediment source and transport

The transition site exhibited a lower proportion of clockwise-loop events (lower HI) and higher SSC_{max} and SSC_{speed} compared to the snow-dominated site, suggesting the warmer site had an extended

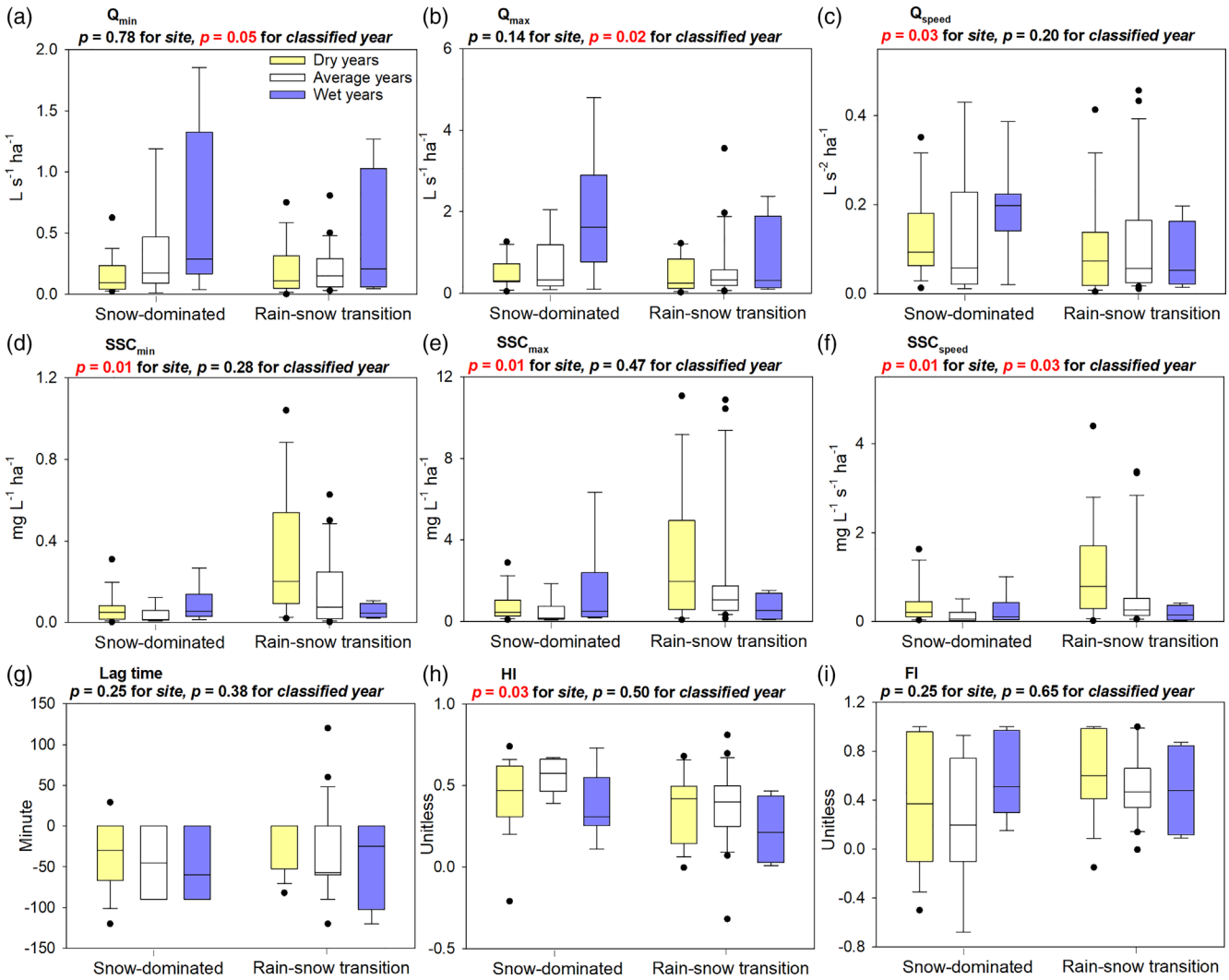

FIGURE 5 Box and whisker plots showing effects of elevation band (snow-dominated and rain-snow transition site) and class of water year (dry, average, or wet) on hysteresis metrics for single peak events at the Kings River Experimental Watersheds. We defined an "average year" as a year with annual precipitation within 30% of the average annual precipitation, a "dry year" that had less than 30% of the average precipitation, and a "wet year" that had at least 30% more precipitation than the average. Each boxplot shows the median value (line), interquartile range (box), 90th and 10th percentiles (tails), and outliers falling outside the 90th and 10th percentiles if they occurred (dots). Significance was determined using nonparametric aligned rank transformation tests with repeated measures (indicated with p values in red when statistically significant at $\alpha = 0.10$)

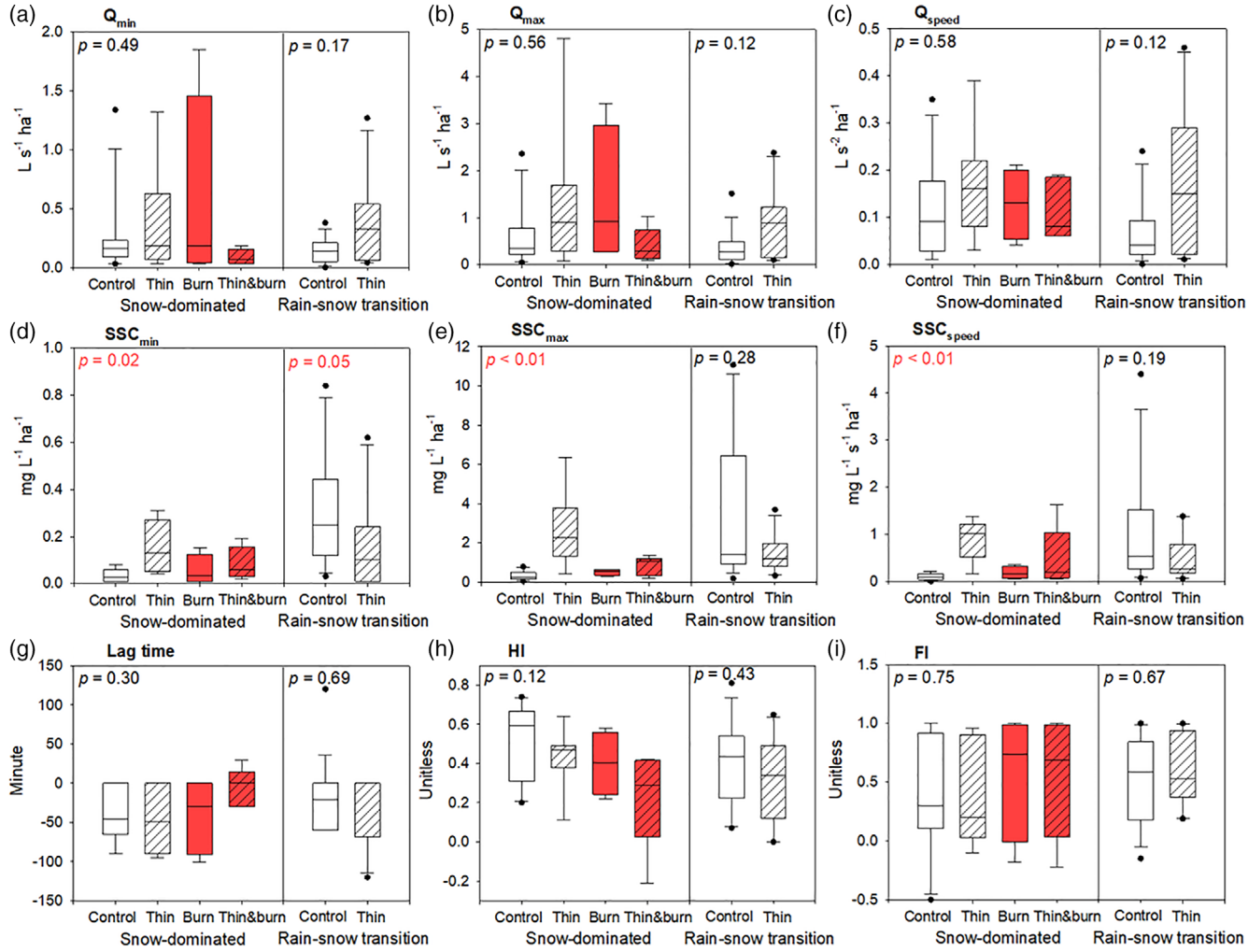

FIGURE 6 Box and whisker plots showing effects of forest thinning and prescribed fire on hysteresis metrics at a higher elevation, snow-dominated site (Bull Creek) and a lower elevation, rain-snow transition site (Providence Creek) at the Kings River Experimental Watersheds in the Southern Sierra Nevada, California. Treatment effects at the snow-dominated site were tested for thin only ($n = 7$), burn only (4), thin combined with burn (5) and control (12). Treatment effects at the transition site were tested for thin only (11) and control (12); burn only and thin combined with burn were not tested at this site because of limited observations (2 and 1, respectively; Table 2). Data were combined across posttreatment water years (WY 2013–2018). Each boxplot shows the median value (line), interquartile range (box), 90th and 10th percentiles (tails), and outliers falling outside the 90th and 10th percentiles if they occurred (dots). Significance was determined using nonparametric aligned rank transformation tests with repeated measures (indicated with p values in red when statistically significant at $\alpha = 0.10$)

sediment source area and greater sediment availability and transport. This may be due to more frequent freeze–thaw cycles that produced areas of greater soil erosion coupled with rain events that increased hydrological connectivity between the sources and the channel (Goudie, 2006; Inamdar et al., 2018; Lopez-Tarazon et al., 2012). Hysteresis analysis in other Mediterranean headwaters also reveals that suspended sediment sources were mostly derived within the channel during snowmelt-related events, but were extended to hillslope sources during rainfall events along with melting snow (Lana-Renault et al., 2011). Climate warming that shifts montane snow-dominated regions to rain-snow transition zones may therefore increase hillslope erosion and downstream sediment delivery.

Similar HI and SSC_{max} were observed amongst years classified as dry, average, and wet, suggesting annual precipitation amounts did not influence sediment source area and event-based sediment transport in our catchments. We observed a higher sediment availability (i.e., SSC_{speed}) in the dry years compared to years with near-average and above average precipitation. The higher sediment availability during the drought period was likely due to soil disaggregation leading to increased erodibility (Buendia et al., 2016; Vermang et al., 2009). Compared to the years with near-average precipitation, decreases in total sediment yield in dry years and increases in sediment yield in wet years have been observed from the same catchments (Safeeq et al., 2022). Therefore, variations in sediment yield amongst years are likely regulated by frequency and duration of precipitation and flow events whilst sediment sources may remain localized across years in our sites in the Southern Sierra Nevada.

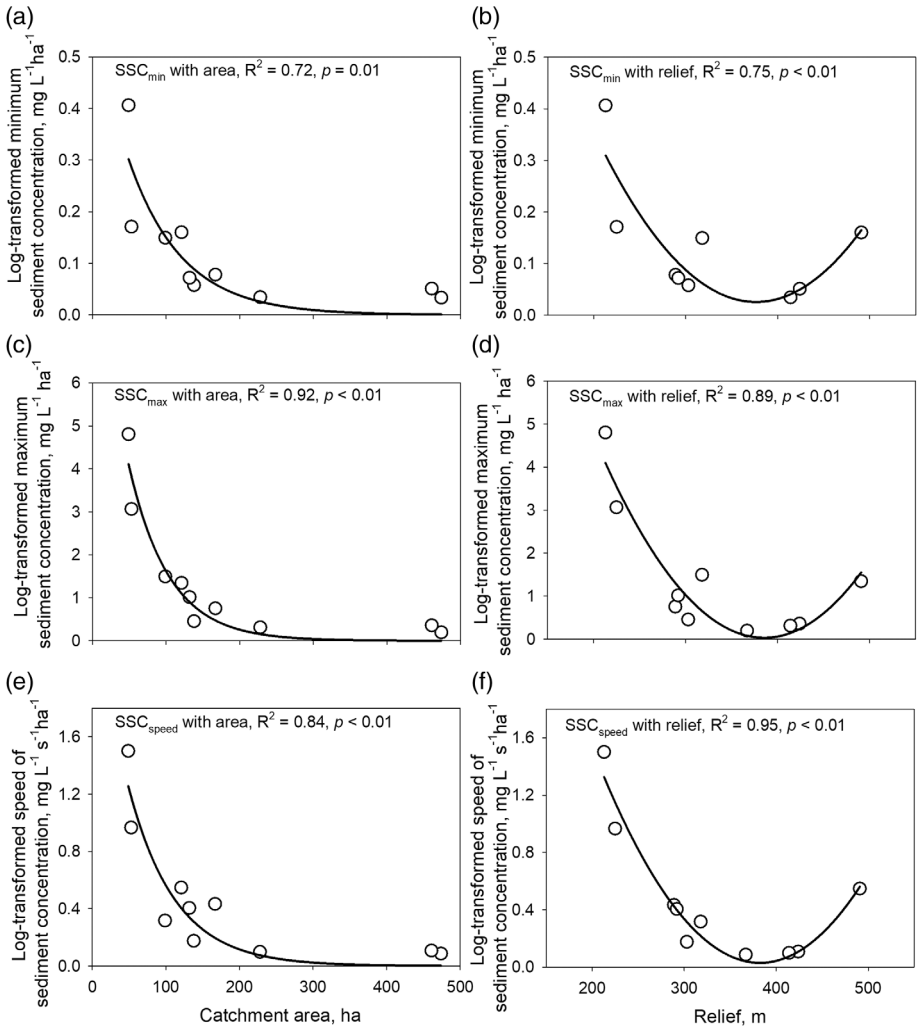

FIGURE 7 The exponential relationships between hysteresis metrics (log-transformed) and catchment area, and the quadratic relationship between hysteresis metrics (log-transformed) and relief at the Kings River Experimental Watersheds: Minimum unit-area suspended sediment concentration (SSC) versus area (a) and relief (b); maximum unit-area SSC versus area (c) and relief (d); and the unit-area SSC_{speed} versus area (e) and relief (f)

4.3 | Impacts of forest thinning and prescribed fire on sediment source and transport

We observed similar HIs from the catchments that received forest thinning and untreated control catchments, suggesting forest thinning did not impact sediment source area in our headwater catchments. We observed differences in SSC_{min}, SSC_{max} and SSC_{speed} between the thin only and control catchments at the two sites (Figure 6), but because the direction of change is not consistent, we attributed these differences to variations in catchment area (Figure 7). The thin only catchment at the snow-dominated site (B201) and the control catchment at the transition site (P304) had higher SSC_{min}, SSC_{max} and SSC_{speed} compared to the other catchments, in part, due to their smaller areas (Figure 7). Our explanation of unchanged sediment transport intensity and availability is further supported by similar SSC_{min}, SSC_{max} and SSC_{speed} between the control catchment and catchment received forest thinning combined with prescribed fire at the snow-dominated site.

The negligible impacts of forest thinning on sediment delivery can be attributed to minor soil-surface disturbances under the low-intensity operations, combined with implementation of best management practises: mechanical equipment was prohibited within 30 m of the streambeds (Lydersen et al., 2019; USDA, 2011). In other montane catchments, the primary sediment source remained in-channels following strip and selective thinning along with road maintenance (Nam et al., 2016; Rachels et al., 2020). However, in thinned catchments that were exposed to heavy machinery for transporting timber, dominant hysteresis patterns changed from clockwise to anti-clockwise following the thinning operation due to increases in hillslope contribution, and then returned to clockwise 5 years later (Kinoshita et al., 2020). In our study catchments, the limited erosion from hillslope and unpaved roads following forest thinning is also attributed to the restricted number of flow events under the confounding drought period; drought occurred immediately following our thinning treatment in 2012 and lasted for nearly 4 years (WY 2013–2016). Hillslope erosion and sediment delivery can be substantial if an intense precipitation occurs following the thinning treatment (e.g., Nam et al., 2016).

None of the hysteresis metrics were different between the control catchment and catchments receiving prescribed fire (burn only and burn combined with thinning; Figure 6), suggesting low severity prescribed fire did not impact sediment sources and transport

intensity. This again can be attributed to a combination of low-severity prescribed fire, implementation of best management practises and the confounding drought period (Lydersen et al., 2019; USDA, 2011; Yang et al., 2022). Significant hillslope erosion and sediment transport have been observed under prescribed fire immediately followed by substantial rainfall events (Benavides-Solorio & MacDonald, 2001; Pierson et al., 2009). In contrast, slope steepness likely plays a minimum role in controlling sediment transport following prescribed fire in montane headwater catchments, as increases in sediment transport were negligible on steep slopes even after high-severity prescribed fire and wildfire (Harrison et al., 2016; Robichaud et al., 2010).

5 | CONCLUSIONS

We examined the effects of the proportion of precipitation that falls as snow, annual precipitation, management operations and physiography on sediment source and transport using hysteresis analysis on 76 single-peak events from 10 headwater catchments over nine water years in the mixed-conifer zone of California's Sierra Nevada. Five catchments from the rain-snow transition site exhibited a lower hysteresis effect and higher sediment availability and transport intensity compared to another five located in the snow-dominated site. This suggests that a warmer climate that shifts precipitation regimes from snow-dominated towards rain-snow transition may increase the chances of multiple sediment sources and event-based transport intensity. Sediment source areas may remain localized across years despite changes in annual precipitation, whereas sediment availability may increase during drought years compared to years with near-average and relatively high precipitation. During the drought period, changes in sediment source and transport intensity can be negligible in catchments receiving low-intensity management operations using best management practises. Overall, in small montane headwater catchments, sediment source will probably remain localized despite changing precipitation amounts and low-intensity management operations, but source may become more distant and possibly lead to higher sediment yields as the main hydrologic input shifts from snow to rain.

ACKNOWLEDGEMENTS

We thank the Pacific Southwest Research Station of the USDA Forest Service, and the National Science Foundation through its support of the Southern Sierra Critical Zone Observatory (EAR-0725097, 1239521, and 1331939) for funding support. We are grateful to Carolyn Hunsaker and Kevin Mazzocco at the Pacific Southwest Research Station and many colleagues from the Sierra National Forest and University of California, Merced for their assistance in the field and laboratory.

DATA AVAILABILITY STATEMENT

Datasets of discharge rates from 2006 to 2015 are available at: https://www.fs.usda.gov/rds/archive/catalog/RDS-2017-0037. Datasets of discharge rates after 2015 and suspended sediment concentrations during the study period can be obtained via email to either MS or JWW.

CONFILIT OF INTEREST

The authors declare that there are no conflicts of interest regarding the content of this article.

ORCID

Yang Yang https://orcid.org/0000-0002-2760-0992
Mohammad Safeeq https://orcid.org/0000-0003-0529-3925
Joseph W. Wagenbrenner https://orcid.org/0000-0003-3317-5141
Stephen C. Hart https://orcid.org/0000-0002-9023-6943

REFERENCES

Agee, J. K., & Skinner, C. N. (2005). Basic principles of forest fuel reduction treatments. *Forest Ecology and Management*, *211*(1–2), 83–96.

Aich, V., Zimmermann, A., & Elsenbeer, H. (2014). Quantification and interpretation of suspended-sediment discharge hysteresis patterns: How much data do we need? *Catena*, *122*, 120–129.

Allen, P. M., Harmel, R. D., Dunbar, J. A., & Arnold, J. G. (2011). Upland contribution of sediment and runoff during extreme drought: A study of the 1947–1956 drought in the Blackland prairie, Texas. *Journal of Hydrology*, *407*(1–4), 1–11.

Amrhein, V., Greenland, S., & McShane, B. (2019). Scientists rise up against statistical significance. *Nature*, *567*, 305–307.

Ares, M. G., Varni, M., & Chagas, C. (2016). Suspended sediment concentration controlling factors: An analysis for the argentine pampas region. *Hydrological Sciences Journal*, *61*(12), 2237–2248.

Arismendi, I., Groom, J. D., Reiter, M., Johnson, S. L., Dent, L., Meleason, M., Argerich, A., & Skaugset, A. E. (2017). Suspended sediment and turbidity after road construction/improvement and forest harvest in streams of the Trask River watershed study, Oregon. *Water Resources Research*, *53*(8), 6763–6783.

Benavides-Solorio, J., & MacDonald, L. H. (2001). Post-fire runoff and erosion from simulated rainfall on small plots, Colorado Front Range. *Hydrological Processes*, *15*(15), 2931–2952.

Bryan, R. B. (2000). Soil erodibility and processes of water erosion on hillslope. *Geomorphology*, *32*(3–4), 385–415.

Buendia, C., Vericat, D., Batalla, R. J., & Gibbins, C. N. (2016). Temporal dynamics of sediment transport and transient in-channel storage in a highly erodible catchment. *Land Degradation & Development*, *27*(4), 1045–1063.

Burnham, K. P., & Anderson, D. R. (2002). *A practical information-theoretic approach. Model selection and multimodel inference* (2nd ed.). Springer.

Clifton, C. F., Day, K. T., Luce, C. H., Grant, G. E., Safeeq, M., Halofsky, J. E., & Staab, B. P. (2018). Effects of climate change on hydrology and water resources in the Blue Mountains, Oregon, USA. *Climate Services*, *10*, 9–19.

Collins, A. L., Blackwell, M., Boeckx, P., Chivers, C. A., Emelko, M., Evrard, O., Foster, I., Gellis, A., Gholami, H., Granger, S., Harris, P., Horowitz, A. J., Laceby, J. P., Martinez-Carreras, N., Minella, J., Mol, L., Nosrati, K., Pulley, S., Silins, U., … Zhang, Y. (2020). Sediment source fingerprinting: Benchmarking recent outputs, remaining challenges and emerging themes. *Journal of Soils and Sediments*, *20*, 4160–4193.

Collins, A. L., Pulley, S., Foster, I. D., Gellis, A., Porto, P., & Horowitz, A. J. (2017). Sediment source fingerprinting as an aid to catchment management: A review of the current state of knowledge and a methodological decision-tree for end-users. *Journal of Environmental Management*, *194*, 86–108.

Diffenbaugh, N. S., Swain, D. L., & Touma, D. (2015). Anthropogenic warming has increased drought risk in California. *Proceedings of the National Academy of Sciences*, *112*(13), 3931–3936.

Duvert, C., Gratiot, N., Némery, J., Burgos, A., & Navratil, O. (2011). Subdaily variability of suspended sediment fluxes in small mountainous catchments — Implications for community-based river monitoring. *Hydrology and Earth System Sciences*, *15*(3), 703–713.

Eder, A., Strauss, P., Krueger, T., & Quinton, J. N. (2010). Comparative calculation of suspended sediment loads with respect to hysteresis effects (in the Petzenkirchen catchment, Austria). *Journal of Hydrology*, *389*(1–2), 168–176.

Esteves, M., Legout, C., Navratil, O., & Evrard, O. (2019). Medium term high frequency observation of discharges and suspended sediment in a Mediterranean mountainous catchment. *Journal of Hydrology*, *568*, 562–574.

Fan, X., Shi, C., Zhou, Y., & Shao, W. (2012). Sediment rating curves in the Ningxia-Inner Mongolia reaches of the upper Yellow River and their implications. *Quaternary International*, *282*, 152–162.

Fang, N. F., Shi, Z. H., Chen, F. X., Zhang, H. Y., & Wang, Y. X. (2015). Discharge and suspended sediment patterns in a small mountainous watershed with widely distributed rock fragments. *Journal of Hydrology*, *528*, 238–248.

Gao, P., & Josefson, M. (2012). Event-based suspended sediment dynamics in a Central New York watershed. *Geomorphology*, *139*, 425–437.

Gao, P., Nearing, M. A., & Commons, M. (2013). Suspended sediment transport at the instantaneous and event time scales in semiarid watersheds of southeastern Arizona, USA. *Water Resources Research*, *49*(10), 6857–6870.

Gomi, T., Dan Moore, R., & Hassan, M. A. (2005). Suspended sediment dynamics in small forest streams of the Pacific northwest 1. *Journal of the American Water Resources Association*, *41*(4), 877–898.

Goudie, A. S. (2006). Global warming and fluvial geomorphology. *Geomorphology*, *79*(3–4), 384–394.

Graham, R. T. (1999). The effects of thinning and similar stand treatments on fire behavior in Western forests. Gen. Tech. Rep. PNW-GTR-463. Portland, OR: U.S. Department of Agriculture, Forest Service, Pacific Northwest Research Station: 27.

Haddadchi, A., & Hicks, M. (2020). Understanding the effect of catchment characteristics on suspended sediment dynamics during flood events. *Hydrological Processes*, *34*(7), 1558–1574.

Haddadchi, A., & Hicks, M. (2021). Interpreting event-based suspended sediment concentration and flow hysteresis patterns. *Journal of Soils and Sediments*, *21*(1), 592–612.

Hamshaw, S. D., Dewoolkar, M. M., Schroth, A. W., Wemple, B. C., & Rizzo, D. M. (2018). A new machine-learning approach for classifying hysteresis in suspended-sediment discharge relationships using high-frequency monitoring data. *Water Resources Research*, *54*(6), 4040–4058.

Harrison, N. M., Stubblefield, A. P., Varner, J. M., & Knapp, E. E. (2016). Finding balance between fire hazard reduction and erosion control in the Lake Tahoe Basin, California–Nevada. *Forest Ecology and Management*, *360*, 40–51.

Henry, H. A. (2008). Climate change and soil freezing dynamics: Historical trends and projected changes. *Climatic Change*, *87*(3), 421–434.

Hunsaker, C. T., & Johnson, D. W. (2017). Concentration-discharge relationships in headwater streams of the Sierra Nevada, California. *Water Resources Research*, *53*(9), 7869–7884.

Hunsaker, C. T., & Safeeq, M. (2018). *Kings river experimental watersheds meteorology data*. Forest Service Research Data Archive. https://doi.org/10.2737/RDS-2018-0028

Hunsaker, C. T., Adair, J., Auman, J., Weidich, K., & Whitaker, T. (2007). *Kings river experimental watershed research study plan* (p. 134p). https://www.fs.fed.us/psw/topics/water/kingsriver/documents/miscellaneous/KREW_Study_Plan_Sep2007.pdf

Hunsaker, C. T., Whitaker, T. W., & Bales, R. C. (2012). Snowmelt runoff and water yield along elevation and temperature gradients in California's southern Sierra Nevada 1. *Journal of the American Water Resources Association*, *48*(4), 667–678.

Inamdar, S., Johnson, E., Rowland, R., Warner, D., Walter, R., & Merritts, D. (2018). Freeze–thaw processes and intense rainfall: The one-two punch for high sediment and nutrient loads from mid-Atlantic watersheds. *Biogeochemistry*, *141*(3), 333–349.

Johnson, D. W., Hunsaker, C. T., Glass, D. W., Rau, B. M., & Roath, B. A. (2011). Carbon and nutrient contents in soils from the kings river experimental watersheds, Sierra Nevada Mountains, California. *Geoderma*, *160*(3–4), 490–502.

Kinoshita, M., Onda, Y., Nam, S., Kato, H., Gomi, T., Chen-wei, C., & Taniguchi, K. (2020). Evaluating of the effect of thinning on suspended sediment runoff in a cypress and cedar plantation forest using Fukushima-derived Cs-137, Cs-134 and Pb-210ex. In EGU General Assembly Conference Abstracts (p. 13119).

Kjelland, M. E., Woodley, C. M., Swannack, T. M., & Smith, D. L. (2015). A review of the potential effects of suspended sediment on fishes: Potential dredging-related physiological, behavioral, and transgenerational implications. *Environment Systems and Decisions*, *35*(3), 334–350.

Klimas, K., Hiesl, P., Hagan, D., & Park, D. (2020). Prescribed fire effects on sediment and nutrient exports in forested environments: A review. *Journal of Environmental Quality*, *49*(4), 793–811.

Klos, P. Z., Link, T. E., & Abatzoglou, J. T. (2014). Extent of the rain-snow transition zone in the western US under historic and projected climate. *Geophysical Research Letters*, *41*(13), 4560–4568.

Lana-Renault, N., Alvera, B., & García-Ruiz, J. M. (2011). Runoff and sediment transport during the snowmelt period in a Mediterranean high-mountain catchment. *Arctic, Antarctic, and Alpine Research*, *43*(2), 213–222.

Langlois, J. L., Johnson, D. W., & Mehuys, G. R. (2005). Suspended sediment dynamics associated with snowmelt runoff in a small mountain stream of Lake Tahoe (Nevada). *Hydrological Processes: An International Journal*, *19*(18), 3569–3580.

Leonard, R. L., Kaplan, L. A., Elder, J. F., Coats, R. N., & Goldman, C. R. (1979). Nutrient transport in surface runoff from a subalpine watershed, Lake Tahoe Basin, California. *Ecological Monographs*, *49*(3), 281–310.

Lloyd, C. E., Freer, J. E., Johnes, P. J., & Collins, A. L. (2016). Testing an improved index for analysing storm discharge–concentration hysteresis. *Hydrology and Earth System Sciences*, *20*(2), 625–632.

Lopez-Tarazon, J. A., Batalla, R. J., Vericat, D., & Francke, T. (2012). The sediment budget of a highly dynamic mesoscale catchment: The river Isábena. *Geomorphology*, *138*(1), 15–28.

Lydersen, J. M., Collins, B. M., & Hunsaker, C. T. (2019). Implementation constraints limit benefits of restoration treatments in mixed-conifer forests. *International Journal of Wildland Fire*, *28*(7), 495–511.

López-Moreno, J. I., Gascoin, S., Herrero, J., Sproles, E. A., Pons, M., Alonso-González, E., Hanich, L., Boudhar, A., Musselman, K. N., Molotch, N. P., Sickman, J., & Pomeroy, J. (2017). Different sensitivities of snowpacks to warming in Mediterranean climate mountain areas. *Environmental Research Letters*, *12*(7), 074006.

Malutta, S., Kobiyama, M., Chaffe, P. L. B., & Bonumá, N. B. (2020). Hysteresis analysis to quantify and qualify the sediment dynamics: State of the art. *Water Science and Technology*, *81*(12), 2471–2487.

Mano, V., Nemery, J., Belleudy, P., & Poirel, A. (2009). Assessment of suspended sediment transport in four alpine watersheds (France): Influence of the climatic regime. *Hydrological Processes: An International Journal*, *23*(5), 777–792.

Martin, S. E., Conklin, M. H., & Bales, R. C. (2014). Seasonal accumulation and depletion of local sediment stores of four headwater catchments. *Water*, *6*(7), 2144–2163.

Nam, S., Hiraoka, M., Gomi, T., Dung, B. X., Onda, Y., & Kato, H. (2016). Suspended-sediment responses after strip thinning in headwater catchments. *Landscape and Ecological Engineering*, *12*(2), 197–208.

Olson, J. R., & Hawkins, C. P. (2017). Effects of total dissolved solids on growth and mortality predict distributions of stream macroinvertebrates. *Freshwater Biology*, *62*(4), 779–791.

Pagano, S. G., Rainato, R., García-Rama, A., Gentile, F., & Lenzi, M. A. (2019). Analysis of suspended sediment dynamics at event scale: Comparison between a Mediterranean and an alpine basin. *Hydrological Sciences Journal*, *64*(8), 948–961.

Park, J., Batalla, R. J., Birgand, F., Esteves, M., Gentile, F., Harrington, J. R., Navratil, O., López-Tarazón, J. A., & Vericat, D. (2019). Influences of catchment and river channel characteristics on the magnitude and dynamics of storage and re-suspension of fine sediments in river beds. *Water*, *11*(5), 878.

Pierson, F. B., Moffet, C. A., Williams, C. J., Hardegree, S. P., & Clark, P. E. (2009). Prescribed-fire effects on rill and interrill runoff and erosion in a mountainous sagebrush landscape. *Earth Surface Processes and Landforms*, *34*(2), 193–203.

Rachels, A. A., Bladon, K. D., Bywater-Reyes, S., & Hatten, J. A. (2020). Quantifying effects of forest harvesting on sources of suspended sediment to an Oregon coast range headwater stream. *Forest Ecology and Management*, *466*, 118123.

Robichaud, P. R., Wagenbrenner, J. W., & Brown, R. E. (2010). Rill erosion in natural and disturbed forests: 1. Measurements. *Water Resources Research*, *46*(10), W10506.

Roehl, J. W. (1962). Sediment source areas, delivery ratios and influencing morphological factors. *International Association for Scientific Hydrology Commission of Land Erosion*, *59*, 202–213.

Safeeq, M., & Hunsaker, C. T. (2016). Characterizing runoff and water yield for headwater catchments in the southern Sierra Nevada. *Journal of the American Water Resources Association*, *52*(6), 1327–1346.

Safeeq, M., Grant, G. E., Lewis, S. L., & Staab, B. (2015). Predicting landscape sensitivity to present and future floods in the Pacific northwest, USA. *Hydrological Processes*, *29*(26), 5337–5353.

Safeeq, M., Nanda, A., Wagenbrenner, J. W., Lewis, J., & Hunsaker, C. T. (2022). Climatic and hydrogeomorphic controls on sediment characteristics in the southern Sierra Nevada. *Journal of Hydrology*, *612*, 128300.

Safeeq, M., Shukla, S., Arismendi, I., Grant, G. E., Lewis, S. L., & Nolin, A. (2016). Influence of winter season climate variability on snow–precipitation ratio in the western United States. *International Journal of Climatology*, *36*(9), 3175–3190.

SAS Institute, Inc. (2013). *SAS version 9.4*. Cary, NC: SAS Institute Inc.

Seeger, M., Errea, M. P., Begueria, S., Arnáez, J., Martı, C., & Garcıa-Ruiz, J. M. (2004). Catchment soil moisture and rainfall characteristics as determinant factors for discharge/suspended sediment hysteretic loops in a small headwater catchment in the Spanish Pyrenees. *Journal of Hydrology*, *288*(3–4), 299–311.

Stacy, E. M., Berhe, A. A., Hunsaker, C. T., Johnson, D. W., Meding, S. M., & Hart, S. C. (2019). Stabilization mechanisms and decomposition potential of eroded soil organic matter pools in temperate forests of the Sierra Nevada, California. *Journal of Geophysical Research: Biogeosciences*, *124*(1), 2–17.

Stacy, E. M., Hart, S. C., Hunsaker, C. T., Johnson, D. W., & Berhe, A. A. (2015). Soil carbon and nitrogen erosion in forested catchments: Implications for erosion-induced terrestrial carbon sequestration. *Biogeosciences*, *12*(16), 4861–4874.

Stafford, A. K. (2011). *Sediment production and delivery from hillslopes and forest roads in the southern Sierra Nevada, California* (Master thesis). Retrieved from https://www.nrel.colostate.edu/assets/nrel_files/labs/macdonald-lab/dissertations/Stafford-thesis-31-March-2011.pdf.

Tsyplenkov, A., Vanmaercke, M., Golosov, V., & Chalov, S. (2020). Suspended sediment budget and intra-event sediment dynamics of a small glaciated mountainous catchment in the Northern Caucasus. *Journal of Soils and Sediments*, 20(8), 3266–3281.

USDA. (2011). *Final environmental impact statement for kings river experimental watershed forest health and research project*. High Sierra Ranger District, Available at. https://www.fs.usda.gov/project/?project=30767

Vaughan, M. C., Bowden, W. B., Shanley, J. B., Vermilyea, A., Sleeper, R., Gold, A. J., Pradhanang, S. M., Inamdar, S. P., Levia, D. F., Andres, A. S., Birgand, F., & Schroth, A. W. (2017). High-frequency dissolved organic carbon and nitrate measurements reveal differences in storm hysteresis and loading in relation to land cover and seasonality. *Water Resources Research*, *53*(7), 5345–5363.

Vermang, J., Demeyer, V., Cornelis, W. M., & Gabriels, D. (2009). Aggregate stability and erosion response to antecedent water content of a loess soil. *Soil Science Society of America Journal*, *73*(3), 718–726.

Wagenbrenner, J. W., Dralle, D. N., Safeeq, M., & Hunsaker, C. T. (2021). The kings river experimental watersheds: Infrastructure and data. *Hydrological Processes*, *35*(5), e14142.

Williams, A. P., Seager, R., Abatzoglou, J. T., Cook, B. I., Smerdon, J. E., & Cook, E. R. (2015). Contribution of anthropogenic warming to California drought during 2012–2014. *Geophysical Research Letters*, *42*(16), 6819–6828.

Williams, G. P. (1989). Sediment concentration versus water discharge during single hydrologic events in rivers. *Journal of Hydrology*, *111*(1–4), 89–106.

Wipfli, M. S., Richardson, J. S., & Naiman, R. J. (2007). Ecological linkages between headwaters and downstream ecosystems: Transport of organic matter, invertebrates, and wood down headwater channels 1. *Journal of the American Water Resources Association*, *43*(1), 72–85.

Yang, Y., Berhe, A. A., Hunsaker, C. T., Johnson, D. W., Safeeq, M., Barnes, M. E., McCorkle, E. P., Stacy, E. M., Bales, R. C., Bart, R. R., Goulde, M. L., & Hart, S. C. (2022). Impacts of climate and disturbance on nutrient fluxes and stoichiometry in mixed-conifer forests. *Biogeochemistry*, *158*, 1–20.

Zabaleta, A., Martínez, M., Uriarte, J. A., & Antigüedad, I. (2007). Factors controlling suspended sediment yield during runoff events in small headwater catchments of the Basque Country. *Catena*, *71*(1), 179–190.

How to cite this article: Yang, Y., Safeeq, M., Wagenbrenner, J. W., Asefaw Berhe, A., & Hart, S. C. (2022). Impacts of climate and forest management on suspended sediment source and transport in montane headwater catchments. *Hydrological Processes*, *36*(9), e14684. https://doi.org/10.1002/hyp.14684

APPENDIX A

TABLE A1 Hysteresis metrics and patterns for 76 single peak events across 10 headwater catchments from water year 2007–2009 and 2013–2018 at the Kings River Experimental Watersheds in the Southern Sierra Nevada, California

							Hysteresis metrics[c]									
Site	Catchment	Calendar year	Month and day	Precipitation category[a]	Treatment assignment[b]	Duration, h	Lag time (min)	Q_{min} (L s^{-1} ha^{-1})	Q_{max} (L s^{-1} ha^{-1})	Q_{speed} (L s^{-2} ha^{-1})	SSC_{min} (mg L^{-1} ha^{-1})	SSC_{max} (mg L^{-1} ha^{-1})	SSC_{speed} (mg L^{-1} s^{-1} ha^{-1})	HI	FI	Hysteresis pattern[§]
Snow-dominated, Bull Creek	B203	2009	May 1	Average	Pretreatment	4.0	0	1.19	2.05	0.43	0.12	0.36	0.11	0.56	0.93	C
		2012	Nov 30	Dry	Pretreatment	7.0	−120	0.31	1.26	0.32	0.01	0.34	0.23	0.52	0.06	C
		2014	Feb 26	Dry	Burn	8.1	0	0.03	0.28	0.04	0.03	0.65	0.21	0.31	0.96	C
		2014	Dec 2	Dry	Burn	13.6	−101	0.08	0.28	0.09	0.00	0.28	0.35	0.58	−0.18	C
		2016	Oct 30	Wet	Burn	8.3	−60	0.29	1.57	0.21	0.04	0.50	0.10	0.50	0.51	C
		2017	Apr 18	Wet	Burn	16.0	0	1.85	3.43	0.17	0.15	0.59	0.05	0.22	1.00	C
	B204	2012	Dec 2	Dry	Thin	4.4	0	0.63	0.98	0.22	0.05	0.42	0.16	0.49	0.90	C
		2014	Dec 2	Dry	Thin&burn	20.8	−30	0.04	0.29	0.18	0.02	1.34	1.63	0.42	0.29	C
		2015	Feb 7	Dry	Thin&burn	6.0	0	0.13	0.45	0.06	0.19	0.46	0.05	0.26	1.00	C
		2015	Jul 9	Dry	Thin&burn	2.5	−30	0.07	0.19	0.08	0.12	1.04	0.45	0.41	−0.22	C
		2015	Jul 21	Dry	Thin&burn	5.5	29	0.03	0.09	0.06	0.04	0.21	0.10	−0.21	0.69	A
		2016	Oct 30	Wet	Thin&burn	8.5	0	0.18	1.02	0.19	0.06	1.04	0.20	0.29	0.98	C
	T003	2012	Nov 30	Dry	Control	4.8	0	0.23	0.87	0.35	0.04	0.43	0.15	0.31	0.70	C
		2012	Dec 2	Dry	Control	6.1	0	0.24	1.20	0.24	0.01	0.64	0.16	0.22	1.00	C
		2014	Feb 26	Dry	Control	3.6	0	0.08	0.29	0.10	0.08	0.50	0.21	0.62	0.99	C
		2014	Dec 2	Dry	Control	4.5	−60	0.12	0.34	0.11	0.06	0.78	0.21	0.74	−0.35	C
		2015	Feb 26	Dry	Control	6.1	−67	0.16	0.34	0.08	0.08	0.31	0.08	0.66	−0.50	C
		2015	Jul 21	Dry	Control	2.0	0	0.03	0.05	0.01	0.03	0.08	0.03	0.20	1.00	C
		2016	Mar 4	Average	Control	7.5	−31	0.23	0.36	0.06	0.01	0.17	0.06	0.67	0.19	C
		2016	Oct 16	Wet	Control	4.0	−90	0.04	0.10	0.02	0.05	0.19	0.08	0.73	0.15	C
		2016	Oct 30	Wet	Control	7.5	−90	0.23	0.52	0.11	0.02	0.20	0.11	0.60	0.27	C
		2017	Apr 7	Wet	Control	18.0	−60	1.34	2.36	0.20	0.01	0.24	0.04	0.31	0.33	C
		2017	Nov 27	Average	Control	6.0	−60	0.17	0.29	0.05	0.01	0.14	0.04	0.59	0.09	C
		2018	Jan 6	Average	Control	12.0	0	0.12	0.20	0.01	0.01	0.06	0.00	0.39	0.68	C
	B201	2014	Oct 31	Dry	Thin	8.1	−30	0.03	0.08	0.03	0.20	1.31	1.03	0.47	0.03	C-A-C
		2014	Dec 2	Dry	Thin	5.6	−49	0.07	0.29	0.08	0.08	2.89	1.21	0.43	0.15	C
		2015	Feb 7	Dry	Thin	7.0	−95	0.11	0.37	0.11	0.31	2.24	1.38	0.64	−0.10	C

(Continues)

TABLE A1 (Continued)

Site	Catchment	Calendar year	Month and day	Precipitation category[a]	Treatment assignment[b]	Duration, h	Hysteresis metrics[c]									Hysteresis pattern[§]
							Lag time (min)	Q_{min} (L s^{-1} ha^{-1})	Q_{max} (L s^{-1} ha^{-1})	Q_{speed} (L s^{-2} ha^{-1})	SSC_{min} (mg L^{-1} ha^{-1})	SSC_{max} (mg L^{-1} ha^{-1})	SSC_{speed} (mg L^{-1} s^{-1} ha^{-1})	HI	FI	
		2016	Dec 15	Wet	Thin	9.4	−72	0.29	1.69	0.22	0.13	3.75	1.01	0.38	0.37	C
		2017	Apr 7	Wet	Thin	20.0	0	1.32	4.80	0.39	0.27	6.33	0.65	0.11	0.96	C
		2017	Nov 27	Average	Thin	17.2	−90	0.18	0.90	0.16	0.04	1.86	0.51	0.49	0.20	C
	B200	2014	Dec 2	Dry	Integrate	8.5	−77	0.09	0.31	0.12	0.01	0.22	0.24	0.66	0.63	C
		2015	Feb 7	Dry	Integrate	4.0	−60	0.37	0.73	0.09	0.05	0.14	0.03	0.54	0.37	C
		2016	Oct 30	Wet	Integrate	7.3	−90	0.15	1.62	0.23	0.06	0.27	0.04	0.29	0.73	C
		2017	Nov 27	Average	Integrate	6.0	−90	0.01	0.09	0.02	0.01	0.14	0.03	0.66	−0.68	C
Rain-snow transition, Providence Creek	P301	2012	Nov 30	Dry	Thin	7.0	0	0.33	1.22	0.24	0.24	1.96	0.45	0.17	0.99	C
		2012	Dec 2	Dry	Thin	5.0	0	0.75	1.21	0.15	0.17	0.81	0.13	0.12	0.60	C
		2018	Apr 7	Average	Thin&burn	21.0	−120	0.81	3.55	0.43	0.04	1.72	0.37	0.40	0.60	C
	P303	2007	Mar 20	Dry	Pretreatment	7.5	−82	0.07	0.13	0.01	0.02	0.08	0.02	0.52	0.45	C
		2012	Nov 30	Dry	Pretreatment	2.3	−60	0.18	0.25	0.04	0.16	0.59	0.69	0.55	−0.15	C
		2015	Feb 8	Dry	Pretreatment	3.0	0	0.02	0.04	0.01	0.03	0.18	0.07	0.29	0.88	C
		2015	July 21	Dry	Pretreatment	8.5	0	0.00	0.02	0.00	0.05	3.30	0.65	0.22	1.00	C
		2016	Feb 18	Average	Pretreatment	2.5	−30	0.18	0.53	0.24	0.24	1.06	0.52	0.81	0.56	C
		2017	Nov 17	Average	Burn	6.5	0	0.03	0.06	0.01	0.00	1.75	0.83	0.27	1.00	C
		2017	Nov 27	Average	Burn	4.0	60	0.03	0.05	0.02	0.01	0.14	0.06	−0.32	0.36	A
	P304	2007	Feb 10	Dry	Pretreatment	2.8	0	0.18	0.41	0.12	1.04	4.81	1.98	0.68	1.00	C
		2007	Mar 20	Dry	Pretreatment	3.1	−45	0.15	0.40	0.09	0.09	5.09	2.40	0.43	0.52	C
		2007	Dec 18	Average	Pretreatment	6.3	−60	0.12	0.40	0.09	0.50	10.87	3.37	0.27	0.32	C
		2012	Dec 2	Dry	Control	8.0	−22	0.30	0.79	0.11	0.77	6.87	1.77	0.09	0.98	C
		2014	Feb 26	Dry	Control	7.8	0	0.07	0.33	0.04	0.84	11.07	1.63	0.08	0.93	C
		2014	Dec 2	Dry	Control	4.3	−30	0.05	0.18	0.06	0.45	8.68	4.40	0.42	0.60	C
		2015	Apr 25	Dry	Control	6.5	−19	0.05	0.09	0.01	0.27	1.47	1.20	0.47	0.37	C
		2015	Dec 10	Average	Control	4.1	0	0.04	0.09	0.03	0.14	1.37	0.56	0.55	0.73	C
		2016	Jan 23	Average	Control	7.5	0	0.15	0.28	0.02	0.24	0.87	0.17	0.23	0.69	C
		2016	Feb 17	Average	Control	5.0	−60	0.11	0.52	0.10	0.42	10.43	3.34	0.28	0.63	C
		2016	Apr 9	Average	Control	4.0	−60	0.13	0.19	0.02	0.26	1.16	0.40	0.45	0.16	C
		2017	Nov 27	Average	Control	4.0	0	0.18	0.33	0.07	0.11	1.30	0.08	0.51	0.14	C
		2018	Jan 8	Average	Control	8.0	−60	0.26	0.40	0.06	0.28	2.22	0.47	0.48	0.22	C

TABLE A1 (Continued)

Site	Catchment	Calendar year	Month and day	Precipitation category[a]	Treatment assignment[b]	Duration, h	Hysteresis metrics[c]									Hysteresis pattern[§]
							Lag time (min)	Q_{min} (L s^{-1} ha^{-1})	Q_{max} (L s^{-1} ha^{-1})	Q_{speed} (L s^{-2} ha^{-1})	SSC_{min} (mg L^{-1} ha^{-1})	SSC_{max} (mg L^{-1} ha^{-1})	SSC_{speed} (mg L^{-1} s^{-1} ha^{-1})	HI	FI	
		2018	Mar 13	Average	Control	5.0	−60	0.22	0.28	0.03	0.07	0.69	0.21	0.70	−0.01	C
		2018	Apr 7	Average	Control	18.0	120	0.38	1.51	0.20	0.63	5.20	0.52	0.07	0.57	C-A-C
	P300	2007	Dec 18	Average	Pretreatment	8.0	−57	0.03	0.32	0.06	0.03	0.55	0.17	0.17	0.47	C
		2009	Jan 22	Average	Pretreatment	4.0	0	0.31	0.51	0.07	0.09	0.38	0.10	0.22	1.00	C
		2014	Feb 26	Dry	Integrate	12.1	0	0.10	0.22	0.08	0.10	0.27	0.09	0.26	0.74	C
		2016	Feb 18	Average	Integrate	5.0	−89	0.27	0.62	0.17	0.03	0.47	0.26	0.42	0.59	C-A-C
		2016	Mar 5	Average	Integrate	24.0	−90	0.38	1.27	0.16	0.05	0.62	0.05	0.40	0.37	C
		2016	Oct 28	Wet	Integrate	5.0	0	0.11	0.22	0.04	0.02	0.09	0.02	0.08	0.77	C-A-C
		2016	Oct 30	Wet	Integrate	2.5	−50	0.30	0.41	0.06	0.04	0.11	0.07	0.47	0.09	C
	D102	2007	Feb 10	Dry	Pretreatment	2.5	−61	0.11	0.23	0.07	0.20	0.57	0.59	0.43	0.15	C
		2012	Nov 30	Dry	Thin	3.2	0	0.37	0.88	0.41	0.62	3.69	1.32	0.65	0.53	C
		2012	Dec 2	Dry	Thin	4.5	0	0.54	1.04	0.29	0.46	2.14	1.38	0.00	1.00	S
		2015	Feb 8	Dry	Thin	3.9	−68	0.04	0.11	0.02	0.10	1.62	0.79	0.44	0.22	C
		2016	Oct 28	Wet	Thin	5.5	−120	0.05	0.10	0.01	0.11	0.98	0.42	0.34	0.19	C
		2017	Apr 7	Wet	Thin	18.0	0	1.27	2.38	0.20	0.05	1.52	0.23	0.01	0.87	S
		2017	Nov 17	Average	Thin	8.0	−90	0.06	0.20	0.03	0.01	1.21	0.27	0.37	0.37	C
		2017	Nov 27	Average	Thin	9.0	−30	0.07	0.15	0.04	0.01	0.32	0.17	0.57	0.37	C
		2018	Jan 8	Average	Thin	15.9	−60	0.06	0.26	0.02	0.03	0.52	0.06	0.49	0.40	C
		2018	Apr 7	Average	Thin	17.0	0	0.50	1.97	0.46	0.01	0.88	0.25	0.27	0.94	C

[§]Hysteresis patterns include: clockwise (C), anticlockwise (A), figure eight showing clockwise-anticlockwise-clockwise (C-A-C), and single-valued bending upwards (S).

[a]Each event falls into different water years that received different annual precipitation amounts and were classified into three categories: an "average year" that had annual precipitation between 1046 and 1323 mm (WY 2008, 2009, 2016 and 2018), a "dry year" that had less than 30% of the average precipitation (WY 2007, 2013, 2014 and 2015), and a "wet year" that had at least 30% more than the average precipitation amount (WY 2017).

[b]Forest thinning was applied in 2012 to two catchments at each site (B201 and B204 at the snow-dominated site and P301 and D102 at the rain-snow transition site). Prescribed fire was applied to two catchments at the snow-dominated site (B203 and B204) in 2013 and two watersheds at the transition site (P301 and P303) in 2016. P304 and T003 were control catchments, and P300 and B200 received integrated effects.

[c]Hysteresis metrics include the unit-area minimum, maximum, and speed of discharge and suspended sediment concentration (i.e., Q_{min}, Q_{max}, Q_{speed}, SSC_{min}, SSC_{max} and SSC_{speed}), lag time (defined as the time between SSC_{max} and Q_{max}), hysteresis index (HI) and flushing index (FI; see text for HI and FI calculations). The Q_{speed} and SSC_{speed} were defined as the difference between the minimum and maximum values divided by the time between their occurrences.

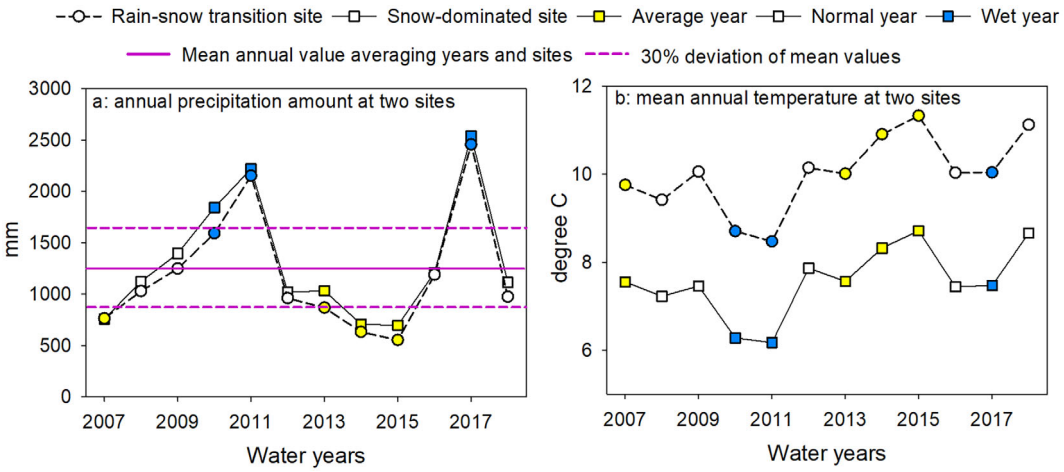

FIGURE A1 Climatic temporal variation within the Kings River Experimental Watersheds in the Southern Sierra Nevada, California. Annual precipitation amount (a) and mean annual air temperature (b) at the snow-dominated site (square symbol) and rain-snow transition site (circle symbol) for water years 2007–2018. Symbols with different colours indicate the classified years based on precipitation levels: Yellow indicates a "dry year" that had 30% below the average precipitation amount or more, white indicates a "average year" that had near-average annual precipitation amount, and blue indicates a "wet year" that had at least 30% above the average precipitation amount or more